JOURNAL OF MATERIALS SCIENCE **39** (2004) 6333–6339

Structural transformation of Al-Fe alloys analysed by neutron diffraction and Mössbauer spectroscopy

S. ENZO
Istituto Nazionale di Fisica della Materia e Dipartimento di Chimica dell'Università di Sassari, via Vienna 2, 07100 Sassari, Italy
E-mail: enzo@ssmain.uniss.it

R. FRATTINI
Istituto Nazionale di Fisica della Materia e Dipartimento di Chimica Fisica dell'Università di Venezia, Dorsoduro 2137, 30123 Venezia, Italy
E-mail: frattini@unive.it

G. MULAS
Istituto Nazionale di Fisica della Materia e Dipartimento di Chimica dell'Università di Sassari, via Vienna 2, 07100 Sassari, Italy

G. PRINCIPI
Istituto Nazionale di Fisica della Materia and Settore Materiali, Dipartimento di Ingegneria Meccanica, via Marzolo 9, 35131 Padova, Italy
E-mail: giovanni.principi@unipd.it

The mechanical treatment of Al-25 at% Fe and Al-34 at% Fe mixtures of pure elemental powders in a high-energy mixer-mill induces solid solution formation and substantial solid state reactivity. Neutron diffraction data were collected over a wide *Q*-range. A quantitative phase evaluation was carried out by the Rietveld method which enabled us to overcome problems of peak overlapping between the two constituent phases. Changes of lattice parameters, as well as lattice strain and average crystallite size were also determined versus the processing time. The local magnetic environment around the iron atoms was simultaneously monitored by means of the Mössbauer spectroscopy.

The formation of an extended bcc solid solution for prolonged treatment times is confirmed even for the present Al-rich compositions.

Neutron diffraction experiments after annealing of the Al-25 at% Fe mechanically alloyed end products revealed a polymorphous phase transformation after 85 min at 583 K, accounting for the metastable character of these materials. The transformation product, Al_5Fe_2, is orthorhombic and stoichiometrically near to the nominal composition. The short interatomic Al-Al distances, resulting from the analysis of the unit cell properties, suggests that oxygen impurities may be present in the system and may play a role for the observed reactivity.

In the case of Al-34 at% Fe composition the products are the Al_5Fe_2 and FeAl intermetallic phases. © *2004 Kluwer Academic Publishers*

1. Introduction

The structural characterization of aluminum-based nanocrystalline alloys is of considerable interest owing to the enhanced physical, electrocatalytic and mechanical properties expected for these new materials [1–3]. Several studies have been devoted to the Fe-Al alloys prepared by mechanical alloying (MA), starting from a mixture of pure elemental powders or mechanical milling (MM), ball milling of a single-phase compound. Studies have been done at different concentration of constituents, especially at the stoichiometric compositions Fe_3Al and FeAl[4–10]. In previous publications [11–13] we reported the structural behaviour and thermal stability of Al-Fe alloys at the stoichiometric compositions, Fe_3Al and FeAl as a function of MA treatment time and of annealing temperature.

For the $Al_{25}Fe_{75}$ and $Al_{50}Fe_{50}$ compositions we have reported a progressive dissolution of aluminum into the bcc α-iron lattice as a function of MA time and the formation of a nanostructured solid solution. In fact, the X-ray diffraction (XRD) patterns showed the gradual disappearance of face centered cubic (fcc) Al peaks

with respect to those of body centered cubic (bcc) iron as a function of mechanical treatment time. The patterns of bcc Fe showed a simultaneous increase of lattice parameter, with broad and asymmetric line profiles in the case of the equiatomic composition [13]. Mössbauer spectroscopy (MS) of the same specimens showed significant changes in the local magnetic environment of the iron atoms. In fact, with increasing MA time, the original magnetic sextet of the starting Fe powder was gradually replaced by a non-magnetic doublet. This behaviour was ascribed to the diffusion of Al atoms in the Fe bcc lattice, with the consequent production of an extended solid solution. A subsequent anneal to 600°C in a differential scanning calorimeter (DSC) displayed exothermic events in the traces that were assigned to the formation of the Fe_3Al and FeAl ordered intermetallics, as detected by XRD. The process of local atomic rearrangements around the iron atoms was also followed by MS, revealing significant changes in the hyperfine parameters.

To further study the interdiffusion and alloying process of Al and Fe we prepared Al-rich alloys with composition Al-34 at% Fe and Al-25 at% Fe.

In previous XRD studies [14, 15], the formation of bcc extended solid solutions was observed, despite the Al-rich composition being expected to give fcc solid solutions. However, Bragg peaks in the X-ray patterns of the mechanically alloyed products were broad and asymmetric. Moreover discrepancies exist in the literature research [16] on the interpretation of the alloying kinetics for this system. For this purpose, the usual approach based on XRD, MS and DSC followed previously [14, 15] is supplemented in the present study by Neutron Diffraction. This technique is complementary to X-ray diffraction in terms of absorption and scattering length of elements and gives the opportunity to investigate *in-situ* the transformation process induced by annealing of massive specimens.

2. Experimental

Powder mixtures of Al-25 at% Fe and Al-34 at% Fe were produced by mixing aluminum and iron powders of 99.99 wt% purity. MA was performed for 0–54 h for Al-25 at% Fe in a hardened steel vial with two $^1/_2$-inch-diameter balls, under an inert atmosphere of argon, using a Spex mixer/mill model 8000. Ethanol (0.05 ml/g of powder) was added as a lubricant agent to avoid aluminum sticking to the milling media and to slow down the process for a better evaluation of fine details. Neutron Diffraction measurements were performed at the HRPD instrument of the ISIS RAL laboratory in Chilton (UK). HRPD, the High Resolution Powder Diffractometer, is the highest resolution neutron powder diffractometer of its type in the world. Situated almost 100 m from the ISIS target at the end of a neutron guide, it has an unprecedented resolution in the main backscattering detector bank, with a $\Delta d/d$ resolution of $\sim 4 \times 10^{-4}$. Its effectively constant resolution over the wide d-spacing range available gives it unique power in the study of subtle structural details, for example in phase transitions [17].

The specimen Al-25 at% Fe MA for 54 h was placed in the furnace under vacuum and subjected to annealing at different temperatures *in situ* until 673 K.

X-ray diffraction (XRD) patterns were collected with a Bragg-Brentano powder diffractometer using Cu K_α radiation ($\lambda = 1.54178$ Å) and a graphite monochromator in the diffracted beam.

Both X-ray and neutron diffraction data were analyzed with the Rietveld method[18], using the MAUD code [19]. This program, in a fully automated version, is particularly suited for a quantitative evaluation of phases present in neutron diffraction patterns. The parameters of physical meaning such as lattice constant, phase abundance, average crystallite size and microstrain, are deduced from the full pattern analysis and not by comparative investigation of the peak broadening after analysis for each peak.

The Mössbauer spectra were measured at room temperature using a conventional spectrometer in transmission geometry with a ^{57}Co:Rh source of about 5 mCi. The spectra were analyzed by means of a current minimization routine, referring the isomer shifts to metallic iron.

3. Results and discussion

3.1. As-milled powders

The more significant neutron diffraction patterns of Al-34 at% Fe powders mechanically alloyed for the times indicated are reported in Fig. 1a. The wide range of Q displayed in the figure is obtained by the simultaneous use of two detectors. The patterns of Al-25 at% Fe powders shows a similar trend and are not reported for reasons of brevity.

Both patterns of unmilled powders show, in addition to the Al and Fe major phases, weak peaks emerging from the background, which are not observed in the XRD patterns reported in [14, 15]. The profile shape of the peaks of unmilled powders are very narrow, which is due to the high instrument resolution ΔQ. The slightly asymmetric line profile is typical of the time-of-flight apparatus.

As it can be seen from the bar position reported at the bottom of the Fig. 1 for each phase, the even hkl indices of Al (e.g., 200, 220, etc.) overlap with those of bcc α-Fe. In turn, the only peaks of α-Fe not affected by the overlap are the (321) peak at $Q = 8.19$ Å^{-1} (see Fig. 1b) and the very weak (431) peak at $Q = 12$ Å^{-1}, not reported in the figure for reason of clarity. Note that these peaks were not accessed in our preliminary study [14, 15] of the same specimens conducted with conventional X-ray diffractometry using Cu K_α source.

The weak peaks emerging from the background have been attributed, as reported in the bottom of Fig. 1, to impurities, specifically to magnetite and wustite phases of iron. These phases were not appreciated in parallel X-ray diffraction patterns because oxygen atoms in these compounds are enhancing the phase sensitivity of the neutron diffraction technique in comparison to X-ray [20].The quantitative analysis of phases supplied by the Rietveld method confirms that such impurities have a 2 wt% concentration, which may deserve

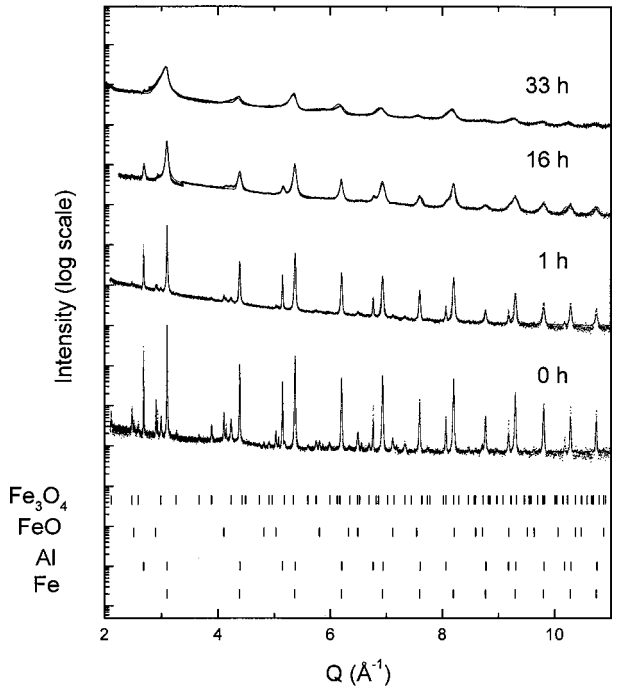

(a)

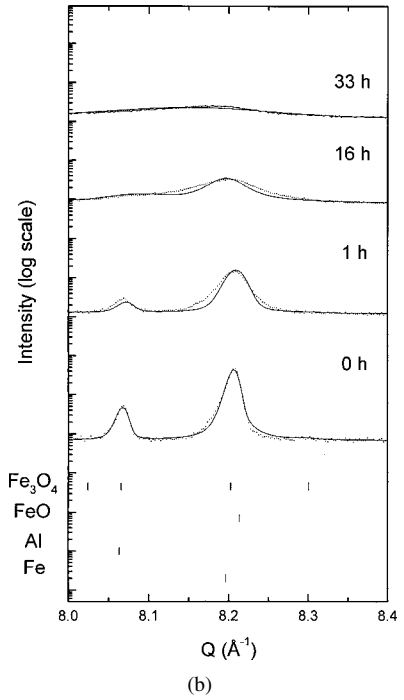

(b)

Figure 1 Neutron diffraction patterns of Al-34 at% Fe (a, b) powders mechanically alloyed for the times indicated. Data points refer to experimental data and full lines to Rietveld fit. The b patterns are a zoom of previous figure made to assess a region where the (321) peak of iron does not overlap with those from aluminum.

some importance for the following mechanically induced solid state reactivity [21].

The mechanical treatment of the powders for different times induces a progressive peak broadening which can be successfully described in our Rietveld fit with the contribution of isotropic size and strain effects. The peaks due to oxide phases are also broadened but persist in the patterns through out the milling treatment.

Average crystallite size and microstrain can thus be deduced with fair degree of confidence from the peak broadening, in spite of unfavorable overlapping of the two major components.

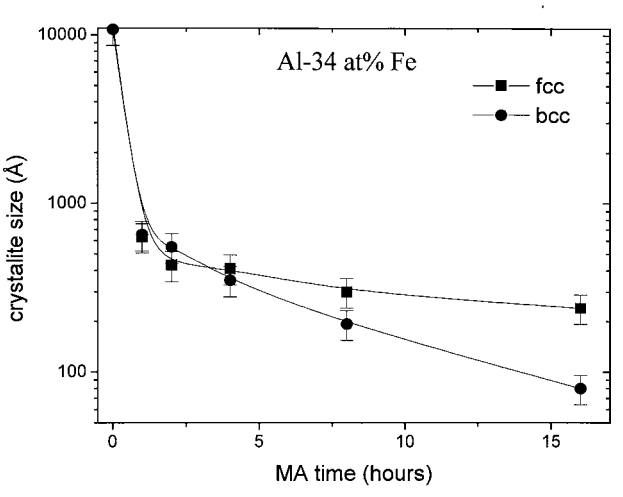

Figure 2 Average crystallite size as a function of milling time for Al-34 at% Fe powders. Full square refers to fcc phase, full circle to bcc phase.

With the present analysis we have extended the Q-range of our previous microstructural analysis based on X-ray diffraction. The new results are reported in Figs 2 and 3 for Al-34 at% Fe composition. The Al-25 at% Fe data are very similar, the only significant difference being at short milling time, since the process appears slightly delayed. As expected the average crystallite size decreases with increasing MA time down to an ultimate value of ca. 100 Å, and the lattice strain increases up to r.m.s values of 7×10^{-3}. It should be noted that in the present Rietveld analysis it is assumed that the Gaussian contribution affects the strain content, while the Cauchian part influences the average crystallite size, which is not the assumption used in the Williamson-Hall [22] and Warren-Averbach [23] methods. This means that different average values of crystallite size and lattice strain can be deduced from the same set of data, according to the approximation involved in the peak shape parametrisation.

With increasing MA time, the peaks of fcc Al that do not overlap with those of iron (e.g., 111, 311, 511, etc.) become weaker and disappear after 33 h of MA

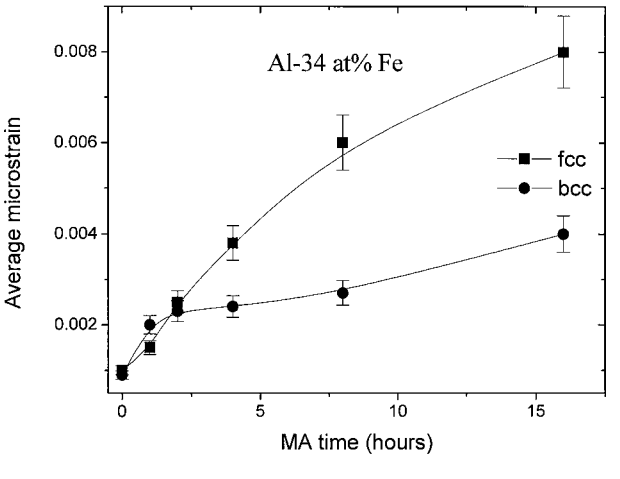

Figure 3 Mean squared lattice strain as a function of milling time for Al-34 at% Fe. Note that in this analysis the strain is evaluated from the gaussian character of peaks.

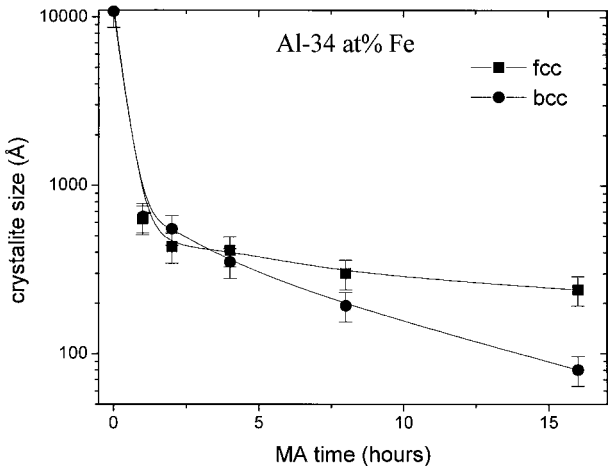

Figure 4 Percentage of fcc phase (full squares) and bcc phase (full circle) as a function of milling time for Al-34 at% Fe powders.

for Al-34 at% Fe composition and after 54 h of MA for the Al-25 at% Fe(see Fig. 4 for Al-34 at% Fe composition). At the end of MA process, essentially all the peaks can be indexed by a bcc structure, as observed previously for equiatomic $Al_{50}Fe_{50}$ and $Al_{25}Fe_{75}$ compositions [14, 15]. We conclude that the product of the mechanical treatment are metastable bcc solid solutions with Al-34 at% Fe and Al-25 at% Fe compositions. Such extended solubility of Al with Fe is ascribed to the ability of the mechanical alloying technique to prepare metastable components in a very wide range of composition.

Fluorescence analysis on the end products indicates a contamination by chromium of ca. 0.4 wt% which suggests a contamination of 3% of steel from the vial.

The Bragg peaks in the final patterns are asymmetric and are broadened anisotropically, which may be ascribed to stacking faults, composition fluctuations and/or the different atomic size of the constituent of the solid solution. This is equivalent to say that such an extended ball milling is not yet sufficient to fully homogenize the solid solution. The same conclusion was also drawn by Yavari *et al.* [10] concerning the $Al_{50}Fe_{50}$ system, after analysis of the (110) peak asymmetry of the XRD pattern. In addition we note that our peak fitting strategy needs further refinement, especially as it concerns the (321) bcc peak profile at 8.19 $Å^{-1}$.

The changes of lattice parameter with respect to the "untransformed" fcc phase can be followed by neutron diffraction with a fair degree of precision because of the presence of 5 not overlapped peaks. As it is reported in Fig. 5a and b, for both compositions, the lattice parameter of fcc Al phase decreases slightly as a function of mechanical treatment time, with a behaviour similar to that reported for $Al_{75}Mo_{25}$ [24, 25]. This suggests the occurrence of Al-Fe extended solid solution during the process of Al consumption, to form the "Al-34 at% Fe" and "Al-25 at% Fe" bcc phases. Conversely, the lattice parameter of the bcc phases (which is built of course on to the geometric habit of α-Fe), increases as a function of the mechanical treatment time. This is also expected on the basis of the atomic size factor ratio of the two constituents.

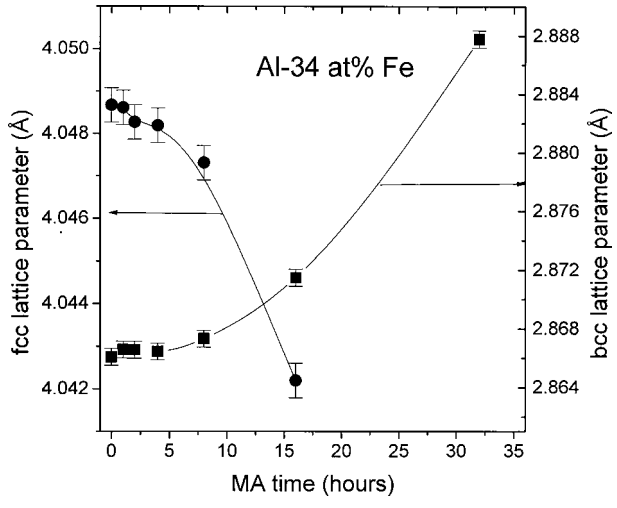

(a)

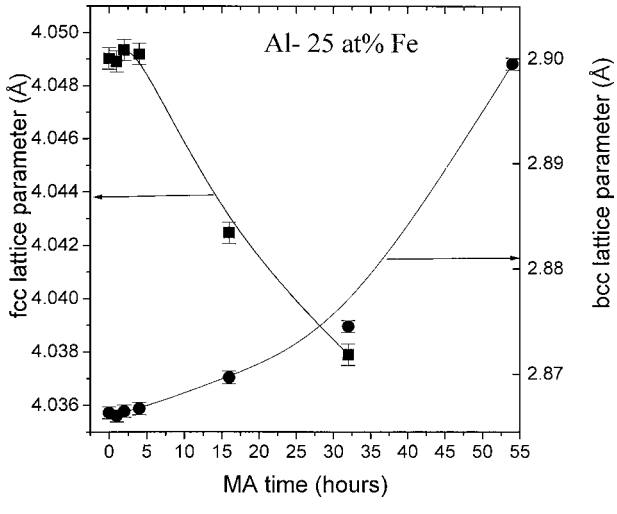

(b)

Figure 5 Lattice parameters of fcc phase and bcc phase, as a function of milling time for Al-34 at% Fe (a) and Al-25 at% Fe (b) powders.

The non-linear lattice parameter change, as a function of mechanical treatment time seems ascribable to complex effects of Al atoms in the bcc lattice.

Mössbauer spectroscopy (MS), which is sensitive to the local atom arrangement around Fe atoms, is shown in Fig. 6a and b for both compositions and provides additional information. The Mössbauer pattern of both sample compositions shows, after 8 h of milling, a main sharp sextet due to unreacted magnetic α-Fe and a weak broad central component ($\delta = 0.45$–0.51 mm/s, $\Gamma = 1.43$–1.60 mm/s, relative area 9–11%) which may correspond to the oxide phases. These phases, detected also in the unmilled powders, can be attributed to the oxides revealed in both specimens by neutron diffraction. Further milling destabilizes the oxide component and reduces the fraction of unreacted iron giving rise to a doublet with parameters (isomer shift $\delta = 0.18$–0.22 mm/s, quadrupole splitting $\Delta = 0.46$ mm/s), typical of iron atoms in an Al rich environment [26], and a weak but significant presence of a broad sextet typical of a bcc Fe(Al) solid solution. The doublet (isomer shift $\delta \cong 0.22$ mm/s, quadrupole splitting $\Delta = 0.54$ mm/s) is the dominant contribution after prolonged milling for both compositions.

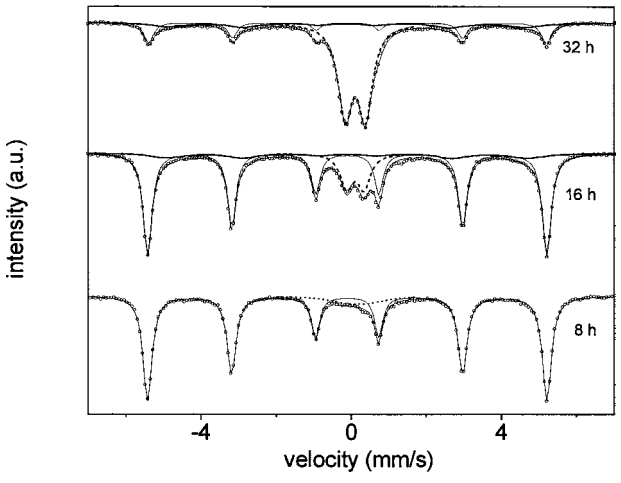

(a)

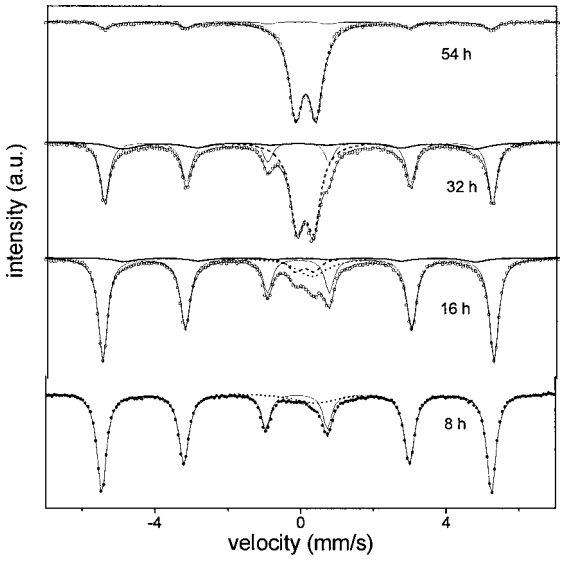

(b)

Figure 6 Transmission room temperature Mössbauer spectra of Al-34 at% Fe (a) and Al-25 at% Fe (b) system mechanically alloyed for the times indicated. Legend of symbols: data points (full circles); best fit (thin solid line); unreacted α-Fe (thin solid line); α-Fe with Al in solid solution (solid thick line); superparamagnetic oxide (dots); Al rich Fe-Al alloy (dash).

It may be worth to conclude that the local magnetic environment of the iron phase is perturbed considerably by the mechanical treatment, to the level of loosing its magnetic identity at room temperature. On the basis of the conclusion by [27], developed only on the Mössbauer analysis, this process can take place either by diffusion of iron atoms into the aluminum remaining matrix or by diffusion of aluminum atoms into the bcc lattice of iron. On the other hand, during the process both the X-ray and Neutron diffraction techniques pointed out to the complete consumption of the fcc Al(Fe) phase and to the increase of the bcc Fe(Al) component at the level of being the only dominant crystallographic phase after prolonged mechanical treatment of 33 and 54 h. Therefore the alloying process may be better described as an intermixing of Al and Fe nanoparticles which are "reacting" to accomplish a bcc structure. Unfortunately, it happens that this bcc structure has a lattice parameter very close to that of unreacted bcc iron, which makes very difficult any effort of evaluating the amount of the newly created Al-Fe bcc phase, even with the sophisticated Rietveld analysis.

3.2. Thermal treatment transformation

Previous DSC annealing experiments up to 873 K [13, 14] were conducted in the calorimeter furnace and the specimens were subjected to XRD and Mössbauer analyses. The structural results, reported in Figs 7 and 8 respectively show that the final products are a mixture of intermetallic AlFe and Al_5Fe_2 phases for Al-34 at% Fe and pure Al_5Fe_2 for Al-25 at% Fe composition. This is evident, from the XRD spectra, by comparing the bar positions at the bottom, while the Mössbauer spectra actually show in the first case a singlet plus a quadrupole doublet, and in the latter just a quadrupole doublet.

In order to enlighten the transformation mechanisms for the MA alloys induced by *in situ* thermal treatment, we report in Fig. 9 the more relevant neutron diffraction patterns. The pattern for the specimen heated up to 523 K shows no difference with the diffraction pattern for the as-milled sample. A transformation from bcc solid solution to a single phase Al_5Fe_2 started to appear after annealing for 85 min at 583 K, and was completed after a 100 min anneal. Longer thermal treatments and at higher temperatures did not produce further phase transformations.

Therefore one transformation step is observed and the occurrence of a single phase for Al-25 at% Fe can

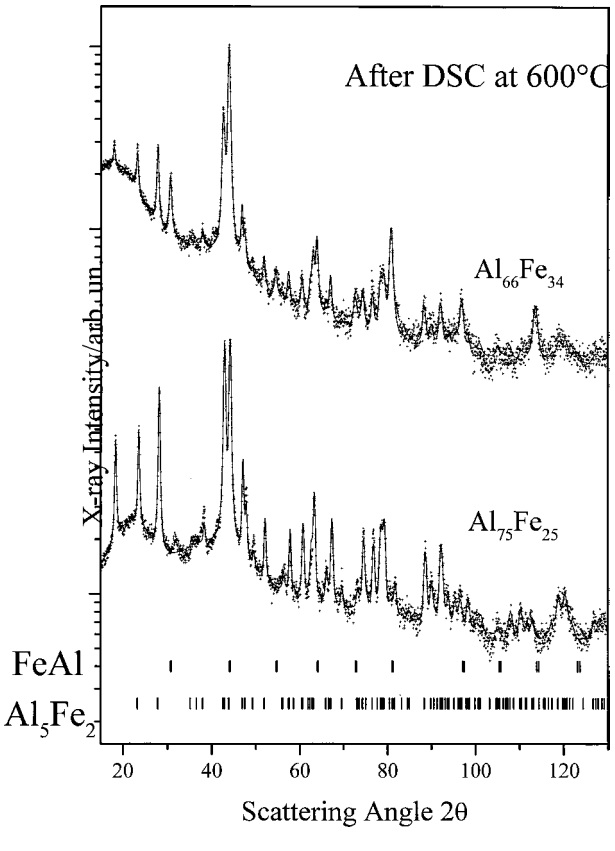

Figure 7 XRD patterns of $Fe_{25}Al_{75}$ and $Fe_{33}Al_{66}$ powders MA for 54 and 32 h respectively after thermal treatment in DSC furnace to 873 K. Data points refer to experiment and full lines to Rietveld fit.

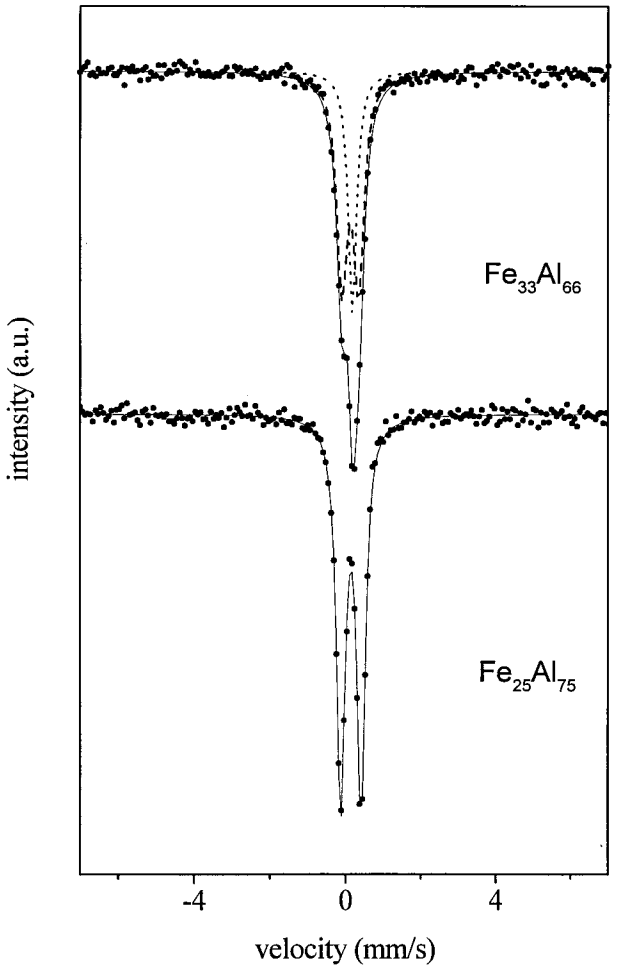

Figure 8 Transmission room temperature Mössbauer spectra of Al-34 at% Fe and Al-25 at% Fe powders mechanically alloyed for 54 and 33 h, respectively, after thermal treatment. Legend of symbols: data points (full circles); best fit (thin solid line); Al rich Fe-Al alloy (dash); ordered B2 phase (dots).

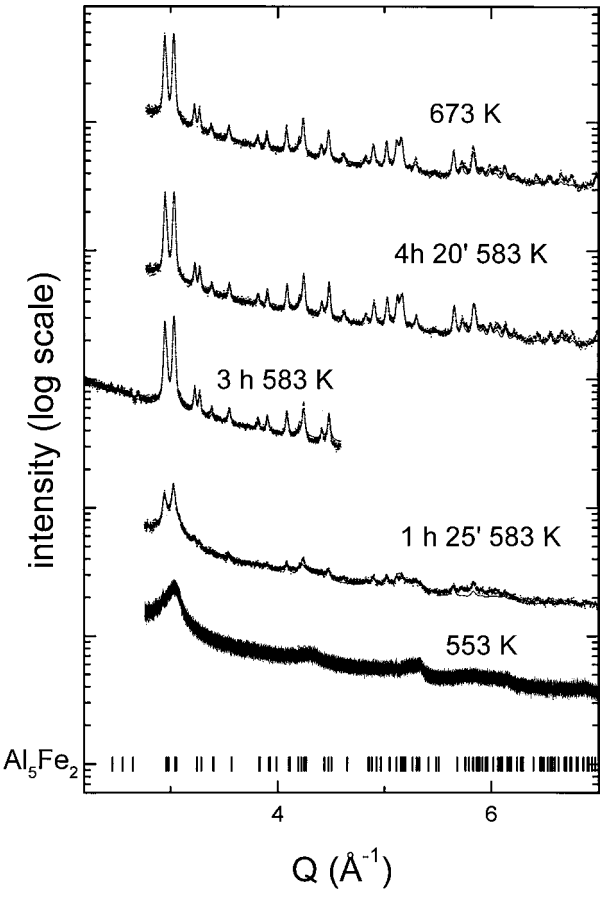

Figure 9 Neutron diffraction patterns of Al-25 at% Fe powder mechanically alloyed for 54 h subjected to annealing at different temperatures *in situ*.

be confirmed. The different sensitivity for iron and aluminum with the neutron radiation with respect to X-rays, enables us to rule out the occurrence of further iron-based phases coexisting after the transformation process.

We note that the orthorhombic unit cell of Al_5Fe_2(space group n. 63 Cmcm, $a = 7.660, b = 6.290, c = 4.196$) is made up by aluminum atom Al_I in positions 8(g) and Al_{II} in positions 4(a), moreover Fe atoms are in position 4(c). Therefore on the base of the total stoichiometry and of the unit cell occupation of the Al_5Fe_2 phase, we are dealing in fact with an "Al_3Fe" phase .

In addition the lattice parameters that we have obtained from the Rietveld analysis for this phase are slightly larger than those just quoted from the literature due to thermal expansion as we collected the data *in situ* at high temperatures.

The fast kinetics of phase transformation suggests a martensitic-type mechanism without appreciable long-range diffusion. This is also confirmed by the evolution of Mössbauer spectra before and after transformation, where the local order parameter do not shows significant changes, testifying negligible variations at the short range scale, meanwhile the lattice structure evolves from cubic to orthorhombic arrangement.

Assuming that the vial was well sealed during the course of the mechanical treatment and that the furnace used for *in situ* annealing during the neutron diffraction experiment was free of atmosphere, oxygen contamination may be originated from just two types of impurities. First we may consider the minor oxide phases visible in the neutron diffraction patterns which amount to ca. 2 wt%. Second we can not disregard the oxygen coming from reduction of the lubricant organic agent, because of the high reactivity of the fresh metal surfaces created by the repeated deformation during mechanical process. As a matter of fact 0.05 ml ethanol/g powder is equivalent to approximately 0.04 mole per mole of Al-25 at% Fe formula units, so that a presence of 4 at% of oxygen in the whole can be justified in the Al_5Fe_2 phase. An indirect confirmation of this come from a weak presence of Fe_3AlC phase (4 wt% according with the Rietveld refinement) in the Al-34 at% Fe specimen annealed at 873 K [15]. It is also possible that *H* atoms of ethanol evolves in the vial as molecular hydrogen or water according to the affinity for oxygen of the Al_5Fe_2 phase. Our LECO analysis for oxygen in the MA products after annealing supplied a figure of 4 at% oxygen, which is compatible with the course of the above mentioned chemical reactions.

It should be noted that the analysis of interatomic distances for the elements of the orthorhombic unit cell supplies a very short Al-Al value (2.11 Å) involving the atoms in position 4(a). We were unsuccessful to reconcile this anomalous short distance with analogous

Al-Al distances that can be found in other aluminum alloys. Thus, we can not disregard the possibility to attribute this effect to some oxygen atoms which were originally present in the system as impurities and go to occupy, at least partially, the 4(a) sites of Al_{II} type atoms.

4. Conclusions

From the present analysis of Al rich compositions it was shown that the occurrence of nanostructured bcc solid solutions is possible despite the fcc structure of the major aluminum component.

In addition, the lattice parameter expansion was limited to a few percent with respect to pure iron, which suggests the introduction of appreciable energetic changes, whose nature is clearly demonstrated by Mössbauer analysis for the local magnetic environment of iron. As a matter of fact, after extended ball milling for both compositions, the initial magnetic sextet is gradually replaced by a non magnetic doublet.

Similar results were also reported in the case of $Al_{75}Mo_{25}$ system [24, 25]. However, in the present case strong asymmetry of the diffraction peaks was evaluated, attributed to the heterogeneity of solid solutions induced by the mechanical treatment. The uncertainty of the previous X-ray diffraction analysis, which showed a high degree of peak overlapping, was overcome by the wider *Q*-range available with neutron diffraction, particularly for what it concerns the iron bcc phase.

The annealing experiments, conducted *in situ*, complemented with Mössbauer data, have shown that the transformation from bcc solid solution to orthorhombic intermetallic Al_5Fe_2 occurs at moderately low temperature via a martensitic-like mechanism, i.e., without long-range diffusion. This transformation happens to be polymorphous in the case of Al-25 at% Fe composition, while it is peritectic in the Al-34 at% Fe, where the FeAl and Al_5Fe_2 compounds coexist at the end of the reaction.

Finally, the role of impurities can not be disregarded for what it concerns the nature of the end products after thermal treatment.

Acknowledgements

The neutron scattering measurements were performed with the support of the Science and Engineering Research Council (RB/7969, RB/7970) and the help of Dr. K. Knight .

Thanks are due to Dr. L. Lutterotti (Università di Trento, Italy) for making available a copy of MAUD code running on a personal computer.

References

1. C. C. KOCH, *Amer. Rev. Mater. Sci. Nanostr. Mater*. **9** (1997) 13.
2. E. GAFFET, *Mater. Trans. Jim* **36** (1995) 198.
3. R. W. SIEGEL and G. E. FOUGERE, in "Nanophase Materials," edited by G. C. Hadjipanais and R. Siegel (Kluwer, Dordrecht, 1994) p. 233.
4. M. A. Morris and D. G. Morris, *Mater. Sci. Forum* **88–90** (1992) 271.
5. T. ZÀK, O. SCHNEIWEISS, Z. COCHNAR and A. BUCHAL, *Mater. Sci. Eng.* **A141** (1991) 73.
6. D. OLESZAK and P. H. SHINGU, *ibid.* **181/182** (1994) 1217.
7. H. SCHROPF, C. KURTH and E. ARTZ, *Scripta Metall. Mater*. **30** (1994) 1569.
8. Y. D. DONG, W. H. WANG, L. LIU, K. Q. XIAO, S. H. TONG and Y. Z. HE, *Mater. Sci. Eng.* **A134** (1991) 867.
9. V. I. FADEEVA, A. V. LEONOV and L. N. KHODINA, *ibid.* **179–181** (1995) 397.
10. A. R. YAVARI, D. NEGRI, E. NAVARRO, A. DERIU, A. HERNANDO and W. J. BOTTA, *Mater. Sci. Forum* **312–314** (1999) 229.
11. E. BONETTI, G. SCIPIONE, G. VALDRÉ, G. COCCO, R. FRATTINI and P. P. MACRÌ, *J. Appl. Phys*. **74** (1993) 2053.
12. E. BONETTI, G. SCIPIONE, R. FRATTINI, S. ENZO and L. SCHIFFINI, *ibid.* **79** (1996) 7537.
13. S. ENZO, R. FRATTINI, R. GUPTA, P. P. MACRÌ, G. PRINCIPI, L. SCHIFFINI and G. SCIPIONE, *Acta Mater*. **44** (1996) 3105.
14. S. ENZO, G. MULAS and R. FRATTINI, *Mater. Sci. Forum* **296–272** (1998) 385.
15. S. ENZO, R. FRATTINI, G. MULAS and F. DELOGU, *ibid.* **296–272** (1998) 391.
16. F. CARDELLINI, V. CONTINI AND G. MAZZONE, *J. Mater. Sci.* **31** (1996) 4175.
17. R. M. IBBERSON, W. I. F. DAVID and K. S. KNIGHT, The High Resolution Neutron Powder Diffractometer (HRPD) at ISIS—A User Guide Report RAL-92-031 (1992).
18. "The Rietveld Method," edited by R. A. Young (International Union of Crystallography, Oxford University Press, Oxford, 1993).
19. L. LUTTEROTTI and S. GIALANELLA, *Acta Mater*. **46** (1998) 101.
20. G. E. BACON, "Neutron Diffraction" (Clarendon Press, Oxford, 1962).
21. N. BURGIO, A. IASONNA, M. MAGINI, S. MARTELLI and F. PADELLA, *Nuovo Cim*. **13D** (1991) 459.
22. G. K. WILLIAMSON and W. H. HALL, *Acta Metall*. **1** (1953) 22.
23. B. E. WARREN and B. L. AVERBACH, *J. Appl. Phys*. **21** (1952) 595.
24. S. ENZO, R. FRATTINI, P. CANTON, G. MULAS and P. RADAELLI, *Nanostr. Mater* **12** (1999) 547.
25. S. ENZO, R. FRATTINI, P. CANTON, M. MONAGHEDDU and F. DELOGU, *J. Appl. Phys*. **87** (2000) 2753.
26. S. NASU, U. GONSER and R. S. PRESTON, *J. de Physique Coll.* **C1** (1980) C1-385.
27. F. CARDELLINI, V. CONTINI, G. MAZZONE and A. MONTONE, *Phil. Mag* **B76** (1997) 629.

Received 12 July 2002
and accepted 23 January 2004